Consistency proof of two denoising methods and the parameter selection of PDE filtering method for ESPI

Zhitao Xiao (肖志涛)[1], Quan Yuan (袁 泉)[1], Fang Zhang (张 芳) [1*], Jun Wu (吴 骏)[1], Lei Geng (耿 磊)[1], Zhenbei Xu (徐振北)[1], and Jiangtao Xi (习江涛)[2]

[1]*School of Electronics and Information Engineering, Tianjin Polytechnic University, Tianjin 300387, China*

[2]*School of Electrical, Computer, and Telecommunications Engineering, University of Wollongong, Wollongong, NSW 2522, Australia*

Corresponding author: hhzhangfang@126.com

Electronic speckle pattern interferometry (ESPI) is a nondestructive, whole-field optical measurement technique. The removal of speckle noise is fundamental to extract measurement information accurately. In this letter, two filtering methods based on the oriented feature of ESPI fringes, i.e., the second-order oriented partial differential equation (SOOPDE) and oriented, regularized quadratic-cost function filtering methods, are first proven to be consistent. An important question in solving partial differential equation, i.e., how to select suitable parameters in an adaptive manner, is then discussed. The computer-simulated and experimentally obtained ESPI fringe patterns and phase map are processed by the SOOPDE filtering model with adaptive selective parameters. The qualitative and quantitative analyses demonstrate that the parameters selected by the adaptive method are effective and suitable for the SOOPDE filtering model.

OCIS codes: 120.6160, 110.6150.

doi: 10.3788/COL201311.121201.

Electronic speckle pattern interferometry (ESPI) is a nondestructive measurement technique that has been applied in numerous areas to measure vibrations, displacements, and their derivatives, as well as to reconstruct three-climensional (3D) objects[1]. With ESPI, useful information is acquired by analyzing ESPI fringe patterns. However, the original ESPI fringe patterns have strong noises. Therefore, effectively denoising fringe patterns is a key problem in applying the ESPI technique.

Orientation is one of the important characteristics of ESPI fringe patterns. In past few decades, several filtering methods based on fringe orientation have been proposed to denoise fringe patterns. Yang *et al.*[2] presented the spin filtering method, which used a curve window to approximate the fringe contour and fitted the gray levels. Villa *et al.*[3] proposed the oriented, regularized quadratic-cost function (ORQCF) method, which used regularization theory in a Bayesian framework to derive a quadratic cost function that includes information about the fringe orientation. Tang *et al.*[4] proposed the second-order oriented partial differential equation (SOOPDE) model to control diffusion orientation. The ORQCF method and the SOOPDE model can provide good filter results to ESPI fringe patterns.

The denoising performance of partial differential equation (PDE) filter methods is related to the parameters used when solving PDE models. These parameters include discrete time step size and iteration number, which are typically chosen by trials. Although Szolgay *et al.*[5] presented the angle deviation error to estimate the ideal stopping condition, only a typical iteration stopping time was provided for the iterative image deconvolution method. This letter discusses how to select the discrete time step size and the iteration number, as well as introduces the correlation coefficient to measure the correlation between signal and noise, which is more direct

and easily understood than the angle deviation error. To harmonize contradiction for denoising and fidelity, the speckle index is also considered as an important standard for selecting filter parameters.

This letter emphasizes the oriented filtering method for ESPI fringe patterns. Firstly, two filtering methods based on the oriented feature of fringes mentioned earlier, i.e., SOOPDE and ORQCF, are proven to be consistent. Secondly, an important question in solving PDE, i.e., how to select suitable parameters such as the discrete time step size and the iteration number, is discussed to obtain an adaptive solution.

ESPI fringe patterns have an obvious oriented feature. Figure 1(a) illustrates a noise-free fringe pattern, and its local region is shown in Fig. 1(b). In Fig. 1(b), the adjacent fringe is approximately parallel, and the fringe orientation varies gradually in the small window. Fringe patterns have a stable orientation when the selected local region is sufficiently small. Figure 1(c) shows the Fourier spectrum of Fig. 1(b). Uniformly distributed fringe patterns transform into two blobs, which are symmetrical around the origin point. The line of the two blobs is
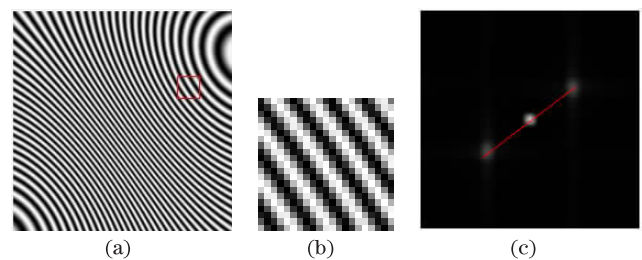

Fig. 1. Pictures of noise-free fringe patterns and the spectrum diagram of its local region. (a) Noise-free fringe patterns, (b) local region of the fringe patterns, and (c) Fourier spectrum of (b).

perpendicular to the fringe orientation. Therefore, the fringe orientation can be calculated based on the position of the blobs.

The ESPI fringe patterns obtained through the experiment are not purely periodic. When formed under an ideal situation, the energy of the blobs will dissipate in the regions with low fringe contrast or massive speckle noise. However, the main frequency energy accounts for most of the energy. The orientation can be calculated by the algorithm presented in Ref. [6] as

$$
\theta_0 = \frac{1}{2}\tan^{-1}\left\{ \frac{\displaystyle\int_\Theta |F(r,\Theta)|^2 \sin(2\Theta)d\Theta}{\displaystyle\int_\Theta |F(r,\Theta)|^2 \cos(2\Theta)d\Theta} \right\}, \quad (1)
$$

where $F(r, \Theta)$ is the Fourier spectrum in a polar form, r is the radial distance from the origin, Θ is the counterclockwise angle from the x axis, and θ_0 denotes the angle between the fringe orientation and the x axis. A 3×3 Gaussian low-pass filter is used to smooth $\theta_0^{[7]}$.

Filtering methods based on PDEs have received considerable research attention in the past few years, which transforms image processing to PDE solving. By introducing fringe oriented information, the diffusion in the SOOPDE is permitted only along the fringe orientation. Therefore, the boundary of the fringe is protected during filtering. Considering the fringe orientation ρ, the SOOPDE model can be expressed as

$$
\partial_t u = \frac{\partial^2 u}{\partial \rho^2} = u_{xx}\cos^2\theta + u_{yy}\sin^2\theta + 2u_{xy}\sin\theta\cos\theta, \quad (2)
$$

where u_{xx}, u_{xy}, and u_{yy} are the second-order partial derivatives of $u(x, y, t)$ with respect to coordinates x and y. The filtered fringe can be obtained through the numerical solution of Eq. (2).

Villa *et al.*[3] proposed a quadratic cost function to denoise fringe patterns. Considering the fringe orientation, the oriented, regularized quadratic-cost function is defined as

$$
U(u_{i,j}) = \sum_{(i,j)\in L}\left\{ (u_{i,j}-I_{i,j})^2 + \mu\left[\left(\frac{\partial u}{\partial \rho}\right)_{i,j}^2 \right.\right.
$$
$$
\left.\left. + \left(\frac{\partial u}{\partial \rho}\right)_{i+1,j}^2 + \left(\frac{\partial u}{\partial \rho}\right)_{i,j+1}^2 \right] \right\}, \quad (3)
$$

where the original image $I_{i,j}$ is the initial condition, μ is a positive constant, and

$$
\left(\frac{\partial u}{\partial \rho}\right)_{i,j} = (u_{i,j}-u_{i-1,j})\cos\theta_{i,j} + (u_{i,j}-u_{i,j-1})\sin\theta_{i,j},
$$

$$
\left(\frac{\partial u}{\partial \rho}\right)_{i+1,j} = (u_{i+1,j}-u_{i,j})\cos\theta_{i+1,j}
$$
$$
+ (u_{i+1,j}-u_{i+1,j-1})\sin\theta_{i+1,j},
$$

$$
\left(\frac{\partial u}{\partial \rho}\right)_{i,j+1} = (u_{i,j+1}-u_{i-1,j+1})\cos\theta_{i,j+1}
$$
$$
+ (u_{i,j+1}-u_{i,j})\sin\theta_{i,j+1}, \quad (4)
$$

In this method, minimizing the cost function is equivalent to smoothing the image only along the fringe orientation, which is implemented by using iterative methods based on the following equation

$$
u^{n+1} - u^n = -\lambda\frac{\partial U}{\partial u}, \quad (5)
$$

where n denotes the iteration number, and λ is an arbitrary positive constant.

Using Eq. (4), the partial derivative of U with respect to u can be expressed as

$$
\left(\frac{\partial U}{\partial u}\right)_{i,j} = 2(u_{i,j}-I_{i,j}) + 2\mu(u_{i,j}-u_{i-1,j})\cos\theta_{i,j}
$$
$$
+ (u_{i,j}-u_{i,j-1})\sin\theta_{i,j}](\cos\theta_{i,j}+\sin\theta_{i,j})
$$
$$
- 2\mu[(u_{i+1,j}-u_{i,j})\cos\theta_{i+1,j} + (u_{i+1,j}
$$
$$
- u_{i+1,j-1})\sin\theta_{i+1,j}]\cos\theta_{i+1,j}
$$
$$
- 2\mu[(u_{i,j+1}-u_{i-1,j+1})\cos\theta_{i,j+1}
$$
$$
+ (u_{i,j+1}-u_{i,j})\sin\theta_{i,j+1}]\sin\theta_{i,j+1}. \quad (6)
$$

Equation (6) can be rewritten and arranged as

$$
\left(\frac{\partial U}{\partial u}\right)_{i,j} = 2(u_{i,j}-I_{i,j}) - 2\mu\left[-\left(\frac{\partial u}{\partial \rho}\right)_{i,j}\right.
$$
$$
\cdot(\cos\theta_{i,j}+\sin\theta_{i,j}) + \left(\frac{\partial u}{\partial \rho}\right)_{i+1,j}
$$
$$
\left.\cdot\cos\theta_{i+1,j} + \left(\frac{\partial u}{\partial \rho}\right)_{i,j+1}\sin\theta_{i,j+1}\right]
$$
$$
= 2(u_{i,j}-I_{i,j}) - 2\mu\left\{\left[\left(\frac{\partial u}{\partial \rho}\right)_{i+1,j}\right.\right.
$$
$$
\left.\cdot\cos\theta_{i+1,j} - \left(\frac{\partial u}{\partial \rho}\right)_{i,j}\cos\theta_{i,j}\right]
$$
$$
\left.+ \left[\left(\frac{\partial u}{\partial \rho}\right)_{i,j+1}\sin\theta_{i,j+1} - \left(\frac{\partial u}{\partial \rho}\right)_{i,j}\sin\theta_{i,j}\right]\right\}
$$
$$
= 2(u_{i,j}-I_{i,j}) - 2\mu\cdot\mathrm{div}\left[\left(\frac{\partial u}{\partial \rho}\right)_{i,j}\right.
$$
$$
\left.\cdot(\cos\theta_{i,j}\widehat{x}+\sin\theta_{i,j}\widehat{y})\right]
$$
$$
= 2(u_{i,j}-I_{i,j}) - 2\mu\cdot\mathrm{div}\left[\left(\frac{\partial u}{\partial \rho}\right)_{i,j}\hat{\rho}\right]
$$
$$
= 2(u_{i,j}-I_{i,j}) - 2\mu\cdot\left(\frac{\partial^2 u}{\partial \rho^2}\right)_{i,j}, \quad (7)
$$

where $\widehat{x}$ and $\widehat{y}$ are the unit vectors with respect to the x and y axis, respectively; and $\widehat{\rho} = \cos\theta\widehat{x}+\sin\theta\widehat{y}$ denotes the unit vector along the fringe orientation.

The iterative process based on Eq. (6) can be rewritten as

$$
\frac{u^{n+1}-u^n}{\lambda} = -\left(\frac{\partial U}{\partial u}\right) = 2\mu\cdot\frac{\partial^2 u}{\partial \rho^2} - 2[u-I]. \quad (8)
$$

Setting $\Delta t = \lambda$, we have

$$\frac{u^{n+1} - u^n}{\lambda} = \frac{u^{n+1} - u^n}{\Delta t} = \partial_t u. \tag{9}$$

Substituting Eq. (9) into Eq. (8) yields

$$\partial_t u = 2(I - u) + 2\mu \cdot \frac{\partial^2 u}{\partial \rho^2}. \tag{10}$$

The first term of Eq. (10) is a fidelity term, the function of which is to assure that the expected solution is insignificantly different from the original image. If the fidelity term is ignored and $\mu = 0.5$, then Eq. (10) will be the same as Eq. (2). That is, the SOOPDE model and the ORQCF method are equivalent. The operational principle of the ORQCF method can be explained further by associating it with the PDE model. The essence of the SOOPDE model is to allow the filtered result to reach the minimal point of the cost function. The operational principle of the two methods demonstrates that the orientation feature of the fringes is important and effective.

The numerical solutions of the PDE provide the filtered images. To compute Eq. (2) numerically, the discrete scheme is given as[8]

$$u_{i,j}^{n+1} = u_{i,j}^n + \Delta t \cdot [(u_{xx})_{i,j}^n \cos^2 \theta_{i,j} + (u_{yy}))_{i,j}^n \sin^2 \theta_{i,j}$$
$$+ 2(u_{xy})_{i,j}^n \sin \theta_{i,j} \cos \theta_{i,j}], \tag{11}$$

where $u_{i,j}^{n+1}$ is the numerical solution, the subscripts i, j denote the pixel position in a discrete two-dimensional (2D) grid, the superscript n denotes the iteration number, the discrete time $t_n = n\Delta t$, and Δt is the time step.

Equation (11) has two key parameters to solve PDE, i.e., the discrete time step size Δt and the iteration number n. Parameters are generally chosen based on trials and errors. Given that the features of the processed image vary, obtaining appropriate parameters for the PDE model may be difficult. Mrázek[9] proposed an adaptive selection method for parameters, which was concerned only with the smoothness of the filtered image and did not consider fidelity in filtering. In this letter, we discuss the influences of the discrete time step size and the iteration number on the performance of solving PDE. Accordingly, a suitable parameter selection method can be obtained. The new method improves[9] by introducing the speckle index to balance denoising and fidelity during filtering.

The diffusion of PDE is shown in Fig. 2. The diffusion filtering starts on the noisy image as its initial condition $u(0) = f$, and the diffusion evolves along a trajectory $u(t)$[9], which depends on the diffusion parameters and the input image.
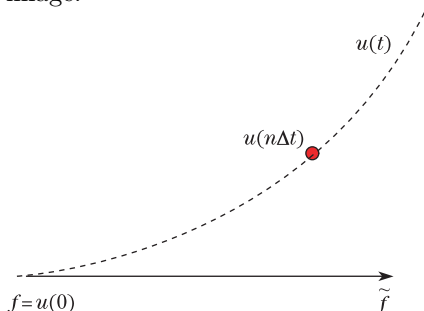

Fig. 2. Schematic of diffusion.

The assumption is that noise will be removed from the data before the important features of the signal commence to deteriorate significantly. In practice, when the filtered image $u(n\Delta t)$ at $t = n\Delta t$ is near the ideal signal $\widetilde{f}$, the correlation of the filtered function $u(n\Delta t)$ and the difference $(u(0) - u(n\Delta t))$ should be smaller. The correlation coefficient of $u(n\Delta t)$ and $(u(0) - u(n\Delta t))$ is defined as[9]

$$\mathrm{corr}(u(0) - u(n\Delta t), u(n\Delta t))$$
$$= \frac{\mathrm{cov}(u(0) - u(n\Delta t), u(n\Delta t))}{\sqrt{\mathrm{var}(u(0) - u(n\Delta t)) \cdot \mathrm{var}(u(n\Delta t))}}, \tag{12}$$

where $\mathrm{cov}(\cdot)$ and $\mathrm{var}(\cdot)$ denote the operation of solving covariance and variance, respectively.

The objective of filtering is to remove noise from fringe patterns. Therefore, the speckle index[10], regarded as a measurement standard for local smoothness of the fringe patterns, should be considered as an important standard for selecting filter parameters. The speckle index is evaluated as the average of the ratios of the local standard deviation to its mean, which is expressed as

$$S = \frac{1}{M \times N} \sum_{i=1}^{M} \sum_{j=1}^{N} \frac{\sigma_{i,j}}{\langle u_{i,j} \rangle}, \tag{13}$$

where $\langle u_{i,j} \rangle$ is the average gray value in the neighborhood for the window with $l \times l$ pixels of the current point, and the local standard deviation $\sigma_{i,j}$ is defined as

$$\sigma_{i,j} = \sqrt{\frac{1}{l^2 - 1} \sum_{k=-1}^{1} \sum_{l=-1}^{1} (u_{i-k,j-l} - \langle u_{i,j} \rangle)^2}. \tag{14}$$

The speckle index can be regarded as an average reciprocal of the signal-to-noise ratio, wherein the signal is the mean value, and the noise is the standard deviation. Therefore, a low speckle index indicates that the local smoothness of the fringe pattern is satisfactory.

Based on the aforementioned theories, the parameters for solving PDE can be selected simply and adaptively.

(1) Selecting the discrete time step size Δt

The degree of smoothness associated with the filtered image is determined by the product of Δt and n. When the product of Δt and n remains constant, similar filtered results will be obtained with different parameters. To reduce operation time, the iteration number should be minimal. Under the condition that the solution of PDE is in a stable region, the time step size Δt should therefore be large. To ensure the convergent solution of PDE, Δt should satisfy the following condition:

$$\mathrm{corr}(u(0) - u(2\Delta t), u(2\Delta t)) < \mathrm{corr}(u(0) - u(\Delta t), u(\Delta t)). \tag{15}$$

Equation (15) indicates that the correlation of signal and noise is decreasing if Δt is suitable.

Hence, Δt can be selected through the following steps.

The initial value is set as $\Delta t_0 = 1$, and the first two filtered results $u(\Delta t_0)$ and $u(2\Delta t_0)$ are computed based on the SOOPDE model. If $\mathrm{corr}(u(0) - u(2\Delta t_0), u(2\Delta t_0)) > \mathrm{corr}(u(0) - u(\Delta t_0), u(\Delta t_0))$, i.e., Eq. (15) is not satisfied, then the current value of Δt is large. Setting $\Delta t_{k+1} = \Delta t_k - 0.05$, the first step is repeated until

Eq. (15) is satisfied. The final value of Δt is the selected discrete time step size.

(2) Selecting the iteration number n

The main objective for selecting n is to make the correlation coefficient of $u(n\Delta t)$ and $(u(0) - u(n\Delta t))$ as low as possible based on the premise that the speckle index of $u(n\Delta t)$ is less than threshold S_0. Firstly, to identify a suitable value for the threshold S_0, 10 computer-simulated, noise-free ESPI fringe patterns with different fringe densities and intensity distributions are tested to compute the speckle index, the mean value of which is used to ensure the local smoothness degree of the fringe patterns. S_0 is set to 0.2. Secondly, using the aforementioned selected value of Δt, the diffusion process is repeated and the values of the two variables, i.e., the speckle index of the filtered function $u(n\Delta t)$ with each n and the correlation coefficient between $u(n\Delta t)$ and the difference of $(u(0) - u(n\Delta t))$, are calculated. Thirdly, n is chosen, in which the following two conditions are satisfied simultaneously:

$$\mathrm{corr}(u(0) - u((n+1)\Delta t), u((n+1)\Delta t)) > \mathrm{corr}(u(0)$$
$$- u(n\Delta t), u(n\Delta t)), \tag{16}$$
$$S < 0.2. \tag{17}$$

When Eqs. (16) and (17) are satisfied, n can be determined. The filtered image based on the adaptive parameters will be obtained simultaneously.

Through experiments, we test the performance of the parameter selection method for the SOOPDE through four aspects. Firstly, computer-simulated ESPI fringe patterns (Fig. 3(a)), which are generated based on the method in Ref. [11], are employed to evaluate the performance of the adaptive parameter selection method for the SOOPDE model. Figure 3 shows the filtered results for the initial ESPI fringe patterns by using the SOOPDE. In addition to the filtered results obtained with the adaptive selective parameters, two filtered images for Fig. 3(a) are provided to demonstrate the validity of the adaptive parameter selection method for the SOOPDE. Two parameters are calculated for each filtered image in Fig. 3. The first is the speckle index S, and the second is the fidelity, which can be defined as

$$F = 1 - \frac{\sum (\widetilde{f} - u)^2}{\sum \widetilde{f}^2}, \tag{18}$$

where $\widetilde{f}$ and u denote the normalized, noise-free fringe image and the filtered fringe image, respectively. A high fidelity value indicates that the processed image is near the noise-free image, i.e., it has a good fidelity.

To evaluate the filtering effect with different iteration numbers, we calculate F and S for each filtered result in Fig. 3, which are given in Table 1. The SOOPDE with the adaptive selective parameters can provide high fidelity and low speckle index. When the speckle index is less than 0.2, the selected iteration number is suitable. The filtering effect with different discrete time step sizes is also evaluated. As mentioned previously, the smoothness degree of the filtered image is determined by the product of Δt and n. By using Fig. 3(c) as an example, the selected discrete time step size Δt and iteration number n are 0.4 and 48, respectively. Several filtered

images for Fig. 3(a), in which the product of Δt and n is approximately equal to 19.2, are therefore obtained. The two evaluation parameters are calculated for these images, which are given in Table 2. The results indicate that when the selected discrete time step size is larger than the adaptive value, the fidelity is small but the speckle index is large, i.e., performance becomes worse. When the discrete time step size is smaller than the adaptive value, the filtered result is close to the adaptive filtered result. To reduce computation time, the iteration number should be small, i.e., the value of Δt should be large based on the condition that the filtered result is sufficient. Therefore, the adaptive discrete time step size selected by our adaptive method is suitable.

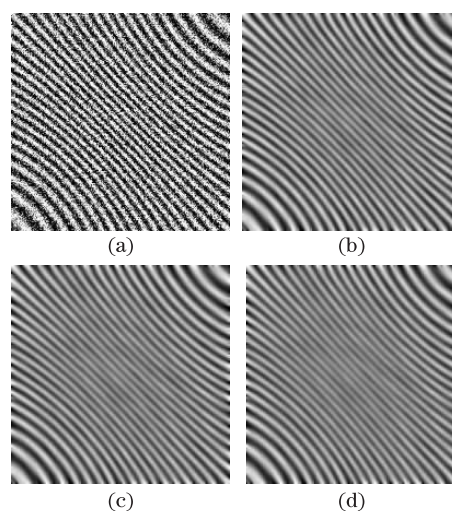Secondly, we study the influences of the speckle and neighbor sizes in Eq. (13) on the performance of the

Fig. 3. Computer-simulated fringe pattern and its filtered image: (a) initial image, (b) filtered image by using the SOOPDE with $\Delta t = 0.4$ and $n = 38$, (c) filtered image by using the SOOPDE with $\Delta t = 0.4$ and $n = 48$, (d) filtered image by using the SOOPDE with $\Delta t = 0.4$ and $n = 58$.

Table 1. Performance Evaluation Results for Different Iteration Numbers Based on the Fringe Patterns Shown in Fig. 3

	Δt	n	F	S
Fig. 3(b)	0.4	38	0.9074	0.2232
Fig. 3(c)	0.4	48	0.8890	0.1984
Fig. 3(d)	0.4	58	0.8717	0.1768

Table 2. Performance Evaluation Results for Different Discrete Time Step Sizes for Fig. 3(a)

Δt	n	F	S
0.2	96	0.8894	0.1988
0.3	64	0.8892	0.1987
0.4	48	0.8890	0.1984
0.5	38	0.8878	0.2042
0.6	32	0.6323	0.2071
0.8	24	0.6259	0.2272

Table 3. Fidelity Comparison Result for Different Speckle Size Noise ESPI Images with the Adaptive Selective Parameters Based on Different Neighbor Sizes in Calculating S

Speckle Size	Window Size in Calculating S					
	3×3		5×5		7×7	
	Parameters	F	Parameters	F	Parameters	F
One	$\Delta t = 0.35$, $n = 38$	0.8854	$\Delta t = 0.35$, $n = 66$	0.8740	$\Delta t = 0.35$, $n = 75$	0.8301
Two	$\Delta t = 0.4$, $n = 28$	0.8734	$\Delta t = 0.4$, $n = 46$	0.8401	$\Delta t = 0.4$, $n = 59$	0.8250
Three	$\Delta t = 0.5$, $n = 16$	0.8658	$\Delta t = 0.5$, $n = 39$	0.8386	$\Delta t = 0.5$, $n = 52$	0.8171

method. Three ESPI images with speckle sizes of one, two, and three pixels are generated by the methods in Refs. [11] and [12]. To select the iteration number n, the neighbor size in Eq. (14) for evaluating $\langle u_{i,j} \rangle$ is set to 3×3, 5×5, and 7×7. Table 3 shows the fidelity comparison result for different speckle sizes of the ESPI images with the adaptive selective parameters based on different neighbor sizes in Eq. (13). The partially filtered images are shown in Fig. 4. The distinct results emerge from the analysis of the numerical tests. As the speckle size increases, a larger Δt is needed to smooth faster and the fidelity becomes lower. The reason for this phenomenon is as follows. Noises exist in the fringe patterns, and thus, the gray levels of some pixels change. Small speckle noises can be removed easily by filters, and the gray levels of such pixels can be recovered. By contrast, large speckle noises are hard to remove and can only be averaged with its neighbors. Therefore, the filtered image that corresponds to small noise ESPI fringe patterns will be more similar to the ideal fringe pattern, i.e., it has higher fidelity. For the same image (i.e., the speckle size is fixed), the iteration number becomes large when a large window is adopted to calculate S to determine the iteration number n, whereas the fidelity becomes low based on the adaptive selective parameters as neighbor size increases when calculating S. Hence, a large iteration number is not always good for denoising, and the 3×3 window for calculating S is sufficiently useful to obtain a suitable iteration number.

Thirdly, experimentally obtained ESPI fringe patterns (Fig. 5(a)) are tested. Figure 5(b) shows the filtered results by using the proposed method. Noises are effectively suppressed by the adaptive SOOPDE model, and the fringe edges are well preserved, even for the high-intensity noise and experimentally obtained ESPI fringe pattern.

Finally, we test the performance of the adaptive parameter selection method on the phase map[13] of ESPI. The wrapped-phase map obtained directly by utilizing the phase-shift procedure is noisy. Filtering for the phase map is necessary and effective during phase extraction. We first calculate the sine and cosine of the wrapped-phase fringe pattern[14], which leads to continuous fringe patterns. The sine and cosine fringe patterns are then filtered individually by using the SOOPDE with the adaptive selective parameters. When the SOOPDE is used for filtering, the adaptive selective parameters for the sine fringe patterns are $\Delta t = 0.3$ and $n = 16$ and those for the cosine fringe patterns are $\Delta t = 0.3$ and $n = 22$. The phase fringe pattern is finally obtained by the inverse tangent of the filtered sine and cosine

fringe patterns. The result is shown in Fig. 6. The filter result can maintain the information of the phase jump while removing the inconsistent dots in the phase pattern effectively.

In conclusion, we conduct an extensive study on filtering methods based on the orientated information for ESPI fringe patterns. We first analyze two commonly used filtering methods, i.e., the SOOPDE filtering method and the ORQCF method, and proved that these two approaches are equivalent. We then propose an
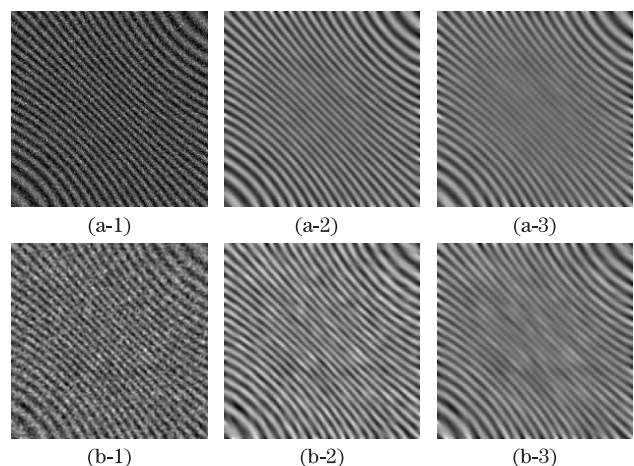

Fig. 4. Two ESPI images with different speckle size and their filtered results: (a-1) and (b-1) are the initial images with speckle noises of one and three pixels, respectively; (a-2) and (a-3) are the filtered images for (a-1) based on the proposed method (which adopt 3×3 and 7×7 windows to calculate S to obtain the iteration number n, respectively); (b-2) and (b-3) are the filtered images for (b-1) based on the proposed method (which adopt 3×3 and 7×7 windows to calculate S to obtain the iteration number n, respectively).
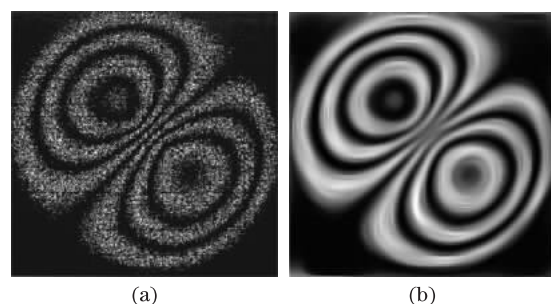

Fig. 5. Experimentally obtained ESPI fringe pattern and its filtered image: (a) initial image, (b) filtered image using the SOOPDE with the adaptive selective parameters $\Delta t = 0.2$ and $n = 137$.
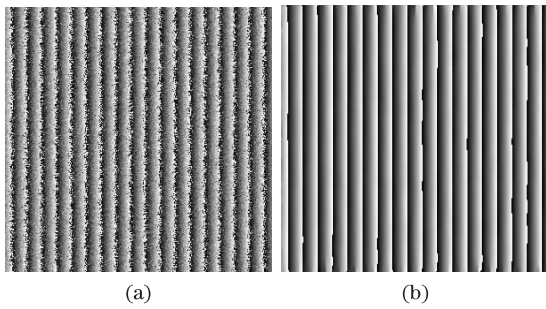
Fig. 6. Phase map of ESPI and its filtered image: (a) initial image, (b) filtered image by using the SOOPDE with the adaptive selective parameters.

adaptive method for selecting parameters to solve the SOOPDE. The performance of the proposed method is tested by two ESPI fringe patterns, i.e., the computer-simulated and experimentally obtained images and the one-phase map of ESPI. The qualitative and quantitative analyses on the filtered results demonstrate that the parameters selected by the adaptive method for the SOOPDE model are effective and suitable for ESPI fringe patterns.

References

1. C. Tang, L. Wang, H. Yan, , and C. Li, Opt. Lasers Eng. **50,** 1036 (2012).
2. X. Yang, Q. Yu, and S. Fu, Opt. Commun. **273,** 60 (2007).
3. J. Villa, J. A. Quiroga, and I. D. L. Rosa, Opt. Lett. **34,** 1741 (2009).
4. C. Tang, L. Han, H. Ren, D. Zhou, Y. Chang, X. Wang, and X. Cui, Opt. Lett. **33,** 2179 (2008).
5. D. Szolgay and T. Szirányi, Electron. Lett. **47,** 442 (2011).
6. S. Chikkerur, A. N. Cartwright, and V. Govindaraju, Pattern Recogn. **40,** 198 (2007).
7. L. Hong, Y. Wan, and A. Jain, IEEE Trans. Pattern Anal. Machine Intell. **20,** 777 (1998).
8. F. Zhang, W. Liu, L. Xia, J. Wang, and Y. Zhu, Chin. Opt. Lett. **7,** 210 (2009).
9. P. Mrázek, "Nonlinear Diffusion for Image Filtering and Monotonicity Enhancement", PhD. Thesis (Czech Technical University, 2001).
10. A. Da'vila, G. H. Kaufmann and D. Kerr, Opt. Eng. **35,** 3549 (1996).
11. X. Zhou, J. P. Baird, and J. F. Arnold, Appl. Opt. **38,** 795 (1999).
12. P. Zhou and K. E. Goodson, Opt. Eng. **40,** 1613 (2001).
13. Z. Xiao, Z. Xu, and F. Zhang, Chin. Opt. Lett. **11,** 101101 (2013)
14. H. Cui, W. Liao, N. Dai, and X. Cheng, Chin. Opt. Lett. **10,** 031201 (2012)